JACS
JOURNAL OF THE AMERICAN CHEMICAL SOCIETY
Article
pubs.acs.org/JACS

Crystalline Graphdiyne Nanosheets Produced at a Gas/Liquid or Liquid/Liquid Interface

Ryota Matsuoka,[†,‡] Ryota Sakamoto,[*,†,§] Ken Hoshiko,[†] Sono Sasaki,[∥,⊥] Hiroyasu Masunaga,[#] Kosuke Nagashio,[§,▽] and Hiroshi Nishihara[*,†]

[†]Department of Chemistry, Graduate School of Science, The University of Tokyo, 7-3-1, Hongo, Bunkyo-ku, Tokyo 113-0033, Japan
[‡]Japan Society for the Promotion of Science (JSPS), Ichibancho, Chiyoda-ku, Tokyo 102-8471, Japan
[§]JST-PRESTO, 4-1-8, Honcho, Kawaguchi, Saitama 332-0012, Japan
[∥]Faculty of Fiber Science and Engineering, Kyoto Institute of Technology,Matsugasaki Hashikami-cho 1, Sakyo-ku, Kyoto 606-8585, Japan
[⊥]RIKEN SPring-8 Center, Hyogo 679-5148, Japan
[#]Japan Synchrotron Radiation Research Institute (JASRI)/SPring-8, 1-1-1 Kouto, Sayo-cho, Sayo-gun, Hyogo 679-5198, Japan
[▽]Department of Materials Engineering, The University of Tokyo, Tokyo 113-8656, Japan

Supporting Information

ABSTRACT: Synthetic two-dimensional polymers, or bottom-up nanosheets, are ultrathin polymeric frameworks with in-plane periodicity. They can be synthesized in a direct, bottom-up fashion using atomic, ionic, or molecular components. However, few are based on carbon−carbon bond formation, which means that there is a potential new field of investigation into these fundamentally important chemical bonds. Here, we describe the bottom-up synthesis of all-carbon, π-conjugated graphdiyne nanosheets. A liquid/liquid interfacial protocol involves layering a dichloromethane solution of hexaethynylbenzene on an aqueous layer containing a copper catalyst at room temperature. A multilayer graphdiyne (thickness, 24 nm; domain size, >25 μm) emerges through a successive alkyne−alkyne homocoupling reaction at the interface. A gas/liquid interfacial synthesis is more successful. Sprinkling a very small amount of hexaethynylbenzene in a mixture of dichloromethane and toluene onto the surface of the aqueous phase at room temperature generated single-crystalline graphdiyne nanosheets, which feature regular hexagonal domains, a lower degree of oxygenation, and uniform thickness (3.0 nm) and lateral size (1.5 μm).

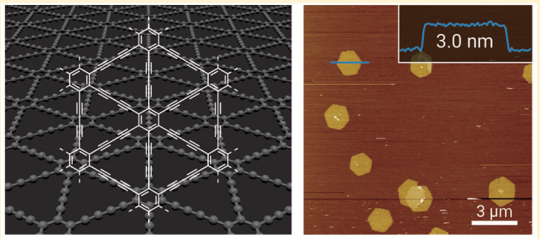

Crystalline Graphdiyne Nanosheet

INTRODUCTION

Two-dimensional (2D) polymers or nanosheets are ultrathin polymeric frameworks with 2D periodicity.[1−4] Nanosheet motifs occur in some bulk crystals and can be exfoliated into individual sheets.[5−8] However, more precise synthesis is possible; nanosheets have been constructed by direct bottom-up methods using atomic, ionic, or molecular components.[9−11] Such methods include 2D network formation on solid surfaces via chemical or physical vapor deposition;[12,13] solvothermal syntheses of imine- or boronate-based covalent organic frameworks (COFs);[14−16] or growing surface metal−organic frameworks (surMOFs) and surface COFs (surCOFs) at solid/liquid,[17−20] liquid/liquid,[21−26] or gas/liquid[21,23,27−29] interfaces. These diverse methods employing a variety of molecular building blocks can provide a wide range of bottom-up nanosheets. However, carbon−carbon bond formation is rarely exploited in 2D nanosheet syntheses, which means that there is a potential new field of investigation into these fundamentally important chemical bonds. Metal-surface-assisted covalent coupling in an ultrahigh vacuum condition is a pioneering strategy to create highly ordered covalent 2D nanostructures.[30−46] This approach can also access 2D motifs unavailable under ambient conditions, though the domain size is limited to 100 nm at most. The photodimerization of anthracene or olefin derivatives in the crystalline phase or at a gas/liquid interface can form synthetic 2D polymers with good crystallinity and large domain sizes,[47−52] but they are susceptible to thermal retrocyclization back to the starting monomers. Aromatic self-assembled monolayers grown on substrates can be converted to carbon nanomembranes via reductive cross-linking upon electron beam irradiation,[53,54] but they are not free from structural disorders. Ultraviolet irradiation of an amphiphilic hexayne monolayer on a gas/water interface can carbonize it to form an sp^2-carbon-rich nanosheet,[55] but the quality of its periodicity has not been fully confirmed.

Given the above background, here we report the liquid/liquid and gas/liquid interfacial syntheses of graphdiyne, a

Received: December 12, 2016
Published: February 15, 2017

DOI: 10.1021/jacs.6b12776
J. Am. Chem. Soc. 2017, 139, 3145−3152

bottom-up covalent nanosheet that incorporates π-conjugated carbon−carbon bonding (Figure 1).[56] Graphdiyne as an allotrope of elemental carbon comprises sp- and sp^2-carbon atoms forming a 2D hexagonal lattice. Li and co-workers reported its bulk synthesis in 2010.[57] They used hexaethynylbenzene (HEB) as a starting monomer, which was dissolved in pyridine in the presence of elemental copper. Copper ions, dissociated from the metallic copper, catalyzed the oxidative homocoupling of HEB, providing graphdiyne in a stacked form that is 1 μm thick. Several subsequent efforts have also sought to create graphdiyne of better quality;[58−61] however, the realization of a thin graphdiyne nanosheet (<10 nm thick) with a defined domain structure and periodicity remains a significant challenge. Our strategy of liquid/liquid or gas/liquid interfacial synthesis affords thin and crystalline graphdiyne at room temperature. Remarkably, the gas/liquid process yields graphdiyne nanosheets as single-crystalline regular hexagonal domains, which feature a low degree of oxygenation and narrow distributions of thickness (as thin as 3 nm) and lateral size (1.5 μm).

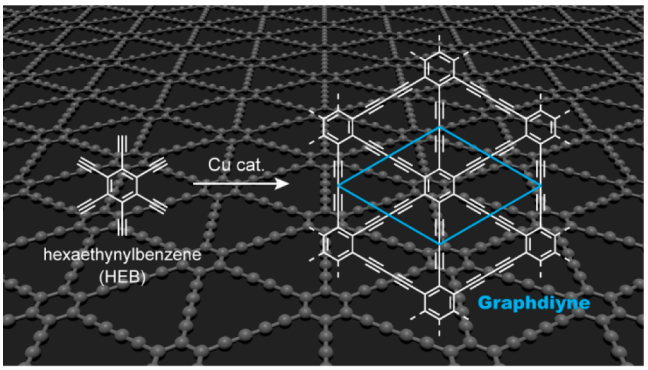

Figure 1. Chemical structure of hexaethynylbenzene (HEB) and graphdiyne.

RESULTS AND DISCUSSION

Liquid/Liquid Interfacial Synthesis of Graphdiyne. We first attempted to produce graphdiyne at the interface between two immiscible liquids (Figure 2a). The upper aqueous layer contained copper(II) acetate and pyridine, which served as a catalyst for acetylenic homocoupling (i.e., Eglinton coupling[62]), and the lower dichloromethane layer contained the HEB monomer. The organic layer was initially overlaid with pure water, which allowed the liquid/liquid interface to remain still while the aqueous solution was added. This process enabled us to circumvent a random encounter between HEB and the catalyst. Under an inert argon atmosphere at room temperature, the successive catalytic coupling reaction for 24 h led to the growth of the 2D covalent network, generating a multilayer graphdiyne film at the liquid/liquid interface (Figure 2b). This dark brown film was insoluble in any solvent, which reflects the π-conjugated polymeric nature of graphdiyne. The as-prepared film was cleaned by replacing each solution with pure solvent; it was then transferred onto flat substrates such as silicon(100) modified with 1,1,1,3,3,3-hexamethyldisilazane [HMDS/Si(100)].

Microscopic Observation of Multilayer Graphdiyne. Optical microscopy of the graphdiyne film generated by the liquid/liquid interfacial synthesis disclosed a sheet morphology with lateral dimensions of 25−100 μm (Figure 2c). Additionally, atomic force microscopy (AFM) revealed its nanoscale morphology (Figure 2d). The film was again shown to be a flat sheet, with a thickness of 24 nm. Therefore, the aspect ratio of the graphdiyne film exceeds 1000. The film also features a stairlike height profile, which indicates the layered structure of the graphdiyne film; the thinner step part has a thickness of 6 nm.

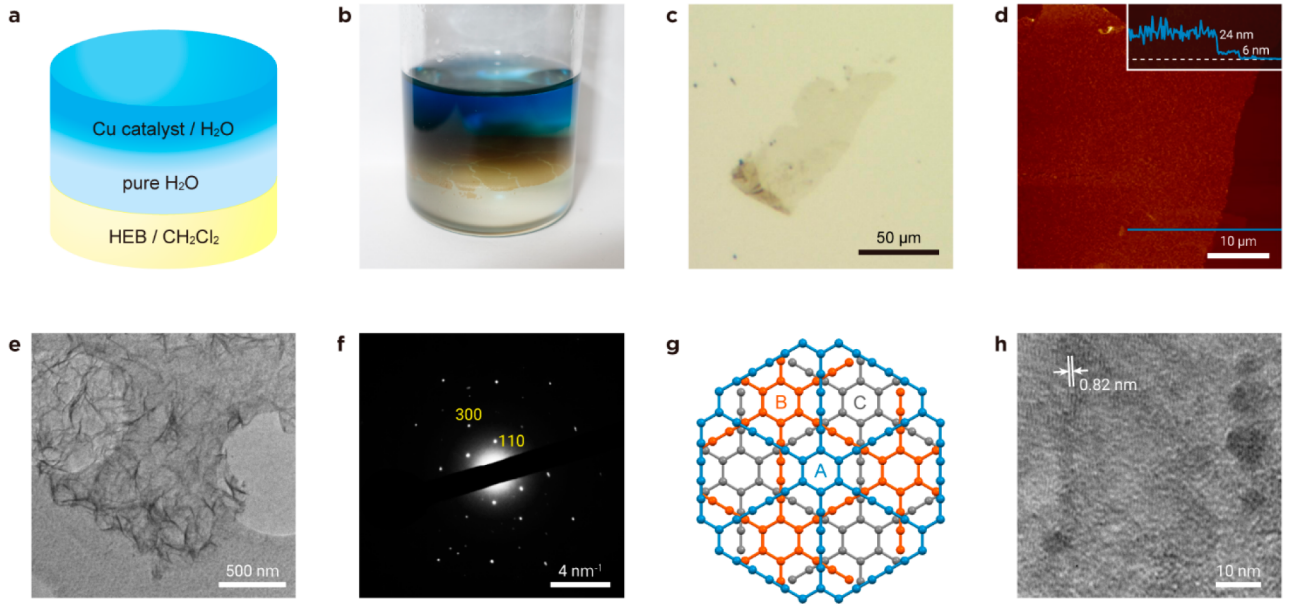

Figure 2. Liquid/liquid interfacial synthesis and microscopic observations of multilayer graphdiyne. Schematic illustration (a) and a photograph (b) of the liquid/liquid interfacial synthetic procedure. (c) Optical microscope image on an HMDS/Si(100) substrate. (d) Atomic force microscope image on HMDS/Si(100) and cross-sectional analysis along the blue line. TEM image (e) and SAED pattern (f) on a holey elastic carbon matrix. Numerical values in panel f denote Miller indices. (g) Graphdiyne lattice of the ABC-stacking configuration (top view) determined by TEM/SAED. (h) High-resolution TEM micrograph.

DOI: 10.1021/jacs.6b12776
J. Am. Chem. Soc. 2017, 139, 3145−3152

2D Periodicity of Multilayer Graphdiyne. Transmission electron microscopy (TEM) and electron diffraction (ED) accompanying the TEM verified the in-plane periodicity of the graphdiyne film obtained at the liquid/liquid interface. Figure 2e shows a typical low-magnification TEM image of the graphdiyne film on a holey carbon matrix. The sheet was sufficiently freestanding to traverse the holes in the carbon matrix. Selected-area ED (SAED) showed a hexagonal pattern (Figure 2f), demonstrating the crystallinity of the graphdiyne film. Comprehensive SAED simulation revealed that the observed diffraction pattern matches exclusively that of A−B−C··· stacking (Figure 2g), excluding the A−A··· and A−B··· stacking structures [Figure S1 in the Supporting Information (SI)]. In this assignment, the innermost hexagonal spot series is indexed as a set of 110 diffractions derived from a hexagonal 2D lattice with $a = b = 0.96$ nm. This value is in good agreement with the theoretical result.[63,64] High-resolution TEM (Figure 2h) showed lattice fringes with an interval of 0.82 nm, which corresponds to the (100) spacing.

Spectroscopic Characterization of Multilayer Graphdiyne. The elemental composition and chemical bonding of multilayer graphdiyne were analyzed by energy-dispersive X-ray spectroscopy (EDS) accompanying scanning electron microscopy (SEM), X-ray photoelectron spectroscopy (XPS), and Raman spectroscopy. For SEM/EDS, the graphdiyne film suspended in ethanol was drop-cast onto a molybdenum grid with a mesh size of 100 μm. EDS point analysis found the presence of three elements (carbon, oxygen, and molybdenum) and the absence of copper (Figure 3a). EDS elemental mapping

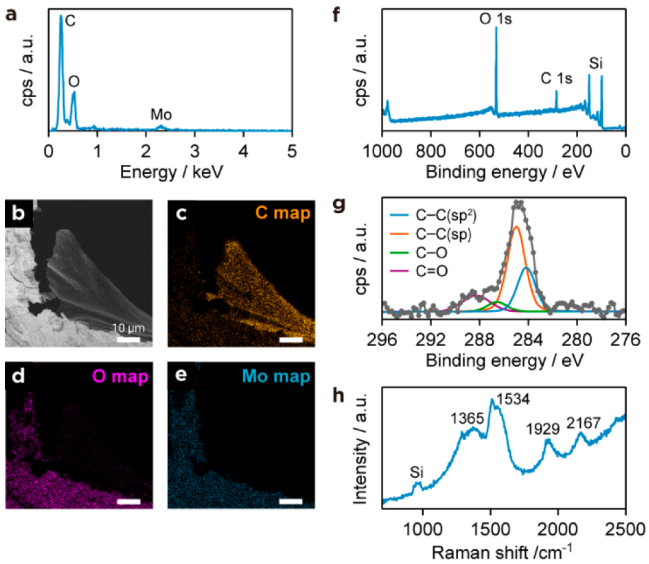

Figure 3. Spectroscopic characterization of multilayer graphdiyne. (a) SEM/EDS at a certain point on a Mo grid. SEM image (b) and SEM/EDS mapping for C (c), O (d), and Mo (e). XPS survey scan (f) and high-resolution C 1s (g) spectra on Si(100). (h) Raman spectrum.

associated with an SEM image (Figure 3b−e) showed carbon to be chiefly located on the film, while oxygen and molybdenum were on the grid, suggesting that the graphdiyne film comprised carbon predominantly. Moreover, carbon was distributed uniformly across the whole sheet, indicating the uniform chemical composition of the sheet. The XPS survey spectrum in Figure 3f displays only a C 1s peak, except for silicon and oxygen signals from the underlying SiO_2 layer grown on the Si(100) substrate. No copper trace was detected therein, which was also confirmed by high-resolution XPS focusing on the Cu 2p region (Figure S2, SI). High-resolution XPS can discern the chemical environment of an element. Here, the C 1s envelope is deconvoluted into four Gaussian curves (Figure 3g), with major contributions from C≡C and C═C species. The abundance ratio of the sp/sp^2 carbons is 2.0, which is in good agreement with the chemical composition of graphdiyne. Minor contributions to the C 1s envelope are ascribable to C−O and C═O species. The calculated oxygen/carbon ratio of 0.21 is comparable to those of graphdiyne samples prepared by other methods (∼0.2)[57,60,61] and of other carbon nanomaterials, such as CVD-grown graphene (∼0.2).[65,66] The presence of sp carbon was also confirmed by Raman spectroscopy (Figure 3h). The spectrum shows four bands typical of graphdiyne: D band (1365 cm^{-1}), G band (1534 cm^{-1}), and two bands derived from the vibration of the conjugated diyne linkage (1929 and 2167 cm^{-1}). Terminal alkyne stretching (2100−2120 cm^{-1}) was not observed at all, which indicates that all the terminal alkyne residues of HEB formed the π-conjugated butadiynyl linkage.

Gas/Liquid Interfacial Synthesis of Graphdiyne. We next sought a better synthesis method to achieve thinner graphdiyne with better quality. Figure 4a illustrates the gas/liquid interfacial synthetic procedure. Herein, a very small amount of HEB (20 nmol) in a mixture of dichloromethane and toluene (220 μL, 1:10 v/v) was gently placed on the surface of an aqueous solution containing the copper catalyst at room temperature under an inert argon atmosphere. The amount of the organic solvent was adjusted such that it spontaneously and quickly evaporated and dissipated. Catalytic polymerization proceeded at the gas/water interface for 24 h, producing a graphdiyne nanosheet that floated on the interface. The graphdiyne nanosheet was invisible to the naked eye but could be transferred onto various flat substrates via a horizontal approach known as the Langmuir−Schäfer method (Figure 4a).

Microscopic Observations of Few-Layer Graphdiyne. The resulting graphdiyne nanosheet was inspected by several microscopic techniques. The existence of the nanosheet domains was confirmed by optical microscopy on HMDS/Si(100) (Figure S3, SI), being visualized as blue dots. To observe them at higher magnification, Figure 4b,c shows typical SEM and TEM micrographs of the graphdiyne nanosheet transferred onto HMDS/Si(100) and an elastic carbon matrix, respectively. The nanosheet domain has a well-defined regular hexagonal shape (measuring 1−2 μm laterally), reminiscent of the hexagonal crystal lattice of graphdiyne. Figure S4a−d (SI) assembles other SEM and TEM images. Among them, Figure S4d shows rolled up nanosheet domains, which demonstrates the polymeric thin film nature of the graphdiyne nanosheet. AFM surveyed the thickness of the hexagonal domain of the nanosheet, as well as its lateral size and surface texture. A representative topograph on HMDS/Si(100) shows several flat and smooth hexagonal domains, with cross-section analysis showing a thickness of 3.0 nm (Figure 4d). This is the thinnest graphdiyne nanosheet to date that we know of. Most of the nanosheet domains have a uniform hexagonal structure [Figures 4d and S5 (SI)]. Thickness data were extracted from 126 independent nanosheet domains; the data exhibited a narrow distribution with two modal values of 2.97 ± 0.03 (major) and 3.94 ± 0.05 nm (minor) (Figure 4e). The difference between the two values (0.97 ± 0.08 nm) corresponds to three layers of graphdiyne (0.34 nm × 3, vide

DOI: 10.1021/jacs.6b12776
J. Am. Chem. Soc. 2017, 139, 3145−3152

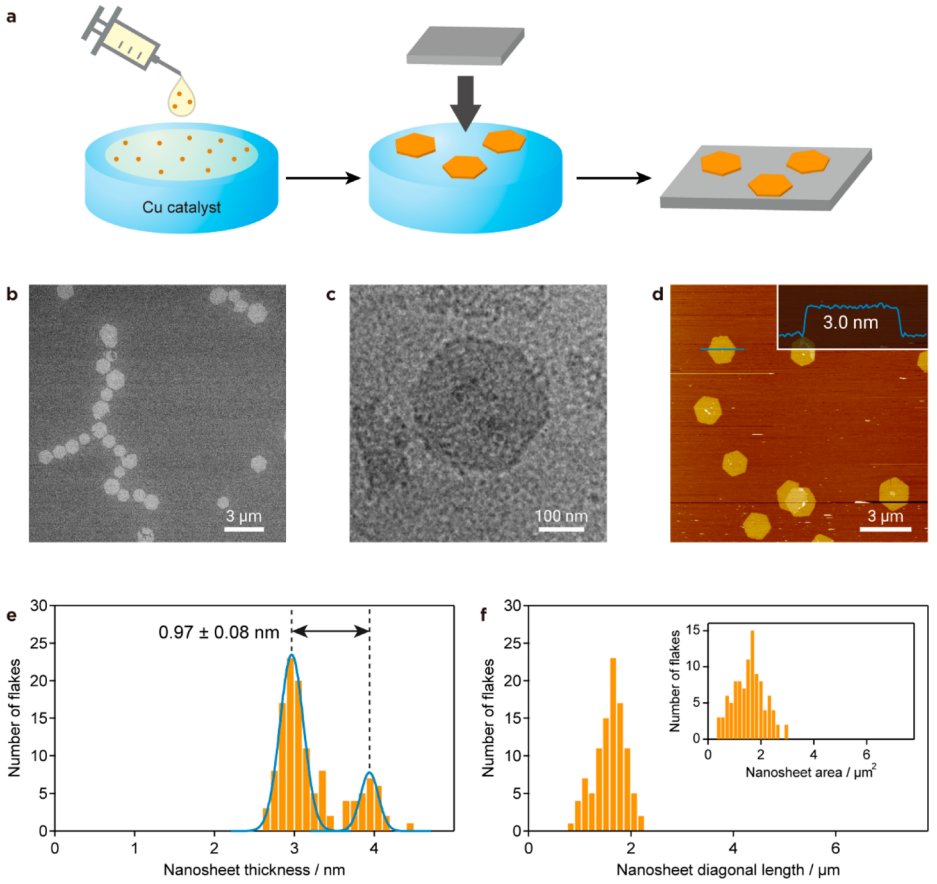

Figure 4. Gas/liquid interfacial synthesis and microscopic observations of few-layer graphdiyne. (a) Schematic illustration of the gas/liquid interfacial synthesis and transfer process. (b) SEM micrograph on HMDS/Si(100). (c) TEM micrograph on an elastic carbon grid. (d) AFM topographic image on HMDS/Si(100) and its cross-sectional analysis along the blue line. (e) AFM thickness histogram (orange bars) and its Gaussian fitting (blue lines). A total of 126 independent hexagonal domains are considered in the histogram. (f) AFM domain size (diagonal length) and domain area (inset) histograms. A total of 101 independent hexagonal domains are considered in the histograms.

infra)—a single unit cell for the ABC-stacking crystal structure (Figure 2g). The hexagonal domains also exhibited a narrow lateral size distribution with an average diagonal length of 1.51 ± 0.30 μm and an average area of 1.55 ± 0.57 μm^2 (Figure 4f). The mean size and area indicate an average of 2 000 000 HEB monomers coupled together in the 2D graphdiyne lattice.

2D Periodicity of Few-Layer Graphdiyne. 2D grazing-incidence wide-angle X-ray scattering (2D GIWAXS) assessed the crystallinity and packing structure of the hexagonal graphdiyne nanosheet. The 2D GIWAXS pattern of 3-nm-thick graphdiyne on HMDS/Si(100) is shown in Figure 5a; it features three diffuse spots along the horizontal and diagonal directions. The solitary horizontal spot, derived from the in-plane periodicity, is assigned to 110 diffraction, while other in-plane diffractions such as 100 and 200 are diminished (Figure 5b, blue plot). Among the three stacking structures considered in the previous section [Figures 2g and S1 (SI)], only the ABC-type stacking reproduces the observed in-plane diffraction pattern (Figure S6, SI). This assignment is consistent with the TEM/SAED result for graphdiyne synthesized by the liquid/liquid interfacial synthesis [Figures 2f and S1 (SI)]. In light of the ABC stacking, the diagonal spots may be indexed as 111 and 201 diffractions derived from a hexagonal lattice with in-plane and out-of-plane periodicities of $a = b = 0.96$ nm and $c = 1.02$ nm, respectively [Figure 5b, orange plot, and Table S1 (SI)]. Again, the a and b lattice constants are consistent with the TEM/SAED result, and the interlayer distance of 0.34 nm

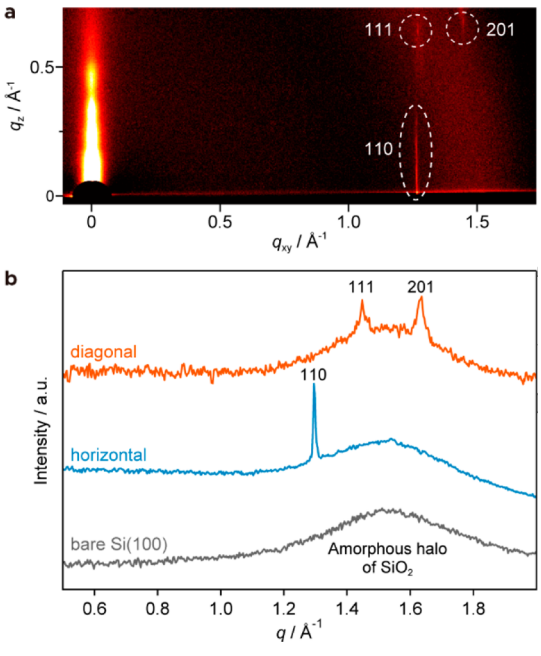

Figure 5. X-ray diffraction profile of few-layer graphdiyne. (a) 2D GIWAXS pattern on Si(100). (b) Horizontal (blue) and diagonal (orange) plots from the 2D GIWAXS pattern shown in panel a. Numerical values denote Miller indices.

DOI: 10.1021/jacs.6b12776
J. Am. Chem. Soc. 2017, 139, 3145−3152

calculated from the c value (i.e., one-third of 1.02 nm) is consistent with those predicted previously for several staggered lattices.[64]

Spectroscopic Characterization of Few-Layer Graphdiyne. Figure 6a shows an XPS survey scan of the hexagonal

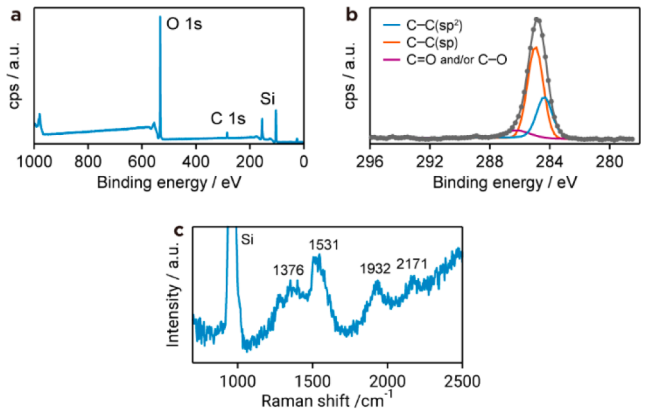

Figure 6. Spectroscopic characterization of few-layer graphdiyne. XPS survey scan (a) and high-resolution C 1s (b) spectra on Si(100). (c) Raman spectrum.

graphdiyne nanosheet on a Si(100) substrate. The spectrum features a C 1s peak derived from graphdiyne, with Si and O peaks derived from the SiO_2 layer of the substrate. No Cu peaks were observed in either survey and narrow scans (Figure S7, SI). This is consistent with the XPS result for multilayer graphdiyne synthesized at the liquid/liquid interface (Figure 3f). However, an XPS narrow scan focusing on C 1s shows a significant difference (Figure 6b): the C 1s envelope can be deconvoluted into three Gaussian fractions, C═O and/or C−O, sp C≡C, and sp^2 C═C. The sp/sp^2 carbon abundance ratio is 2.0, consistent with the chemical composition of graphdiyne. The calculated oxygen/carbon ratio is 0.092, which is notably smaller than values in previous reports (~0.20)[57,60,61] and the ratio found here for multilayer graphdiyne synthesized at the liquid/liquid interface (0.21, Figure 3g). Oxygen passivation is a crucial matter in carbon materials, and the lesser extent of oxygenation, indicative of fewer defects, is thus appreciated. Raman spectroscopy (Figure 6c) found D (1376 cm^{-1}) and G (1531 cm^{-1}) bands and bands from the conjugated diyne linkage (1932 and 2171 cm^{-1}); these bands appeared at wavenumbers similar to those of multilayer graphdiyne (Figure 3h). Therefore, the diffraction and spectroscopic analyses, especially 2D GIWAXS and XPS, confirmed the good crystallinity and low oxygenic defect level of the graphdiyne nanosheet, which is consistent with its regular hexagonal domain shape and its narrow domain size and thickness distributions, as determined by microscopic observations.

CONCLUSIONS

We succeeded in fabricating a π-conjugated covalent 2D nanosheet, graphdiyne, through a carbon−carbon coupling reaction among constitutive monomers (HEB) at a liquid/liquid or gas/liquid interface. The monomer molecules were allowed to react with each other at the liquid/liquid interface generated by an organic solution containing HEB and an aqueous solution of a copper catalyst. The simple biphase combination afforded multilayer graphdiyne, the thickness of which was 24 nm thick, with a step of 6 nm at the edge. TEM and SAED revealed the in-plane periodicity of the multilayer graphdiyne, with an SAED pattern exclusively matching ABC-type stacking. XPS, SEM/EDS, and Raman spectra showed characteristics consistent with the chemical composition and bonding of graphdiyne. The gas/liquid interfacial synthesis performed better than the liquid/liquid synthesis and produced few-layer graphdiyne of higher quality. Microscopic analyses, SEM, TEM, and AFM found well-defined regular hexagonal domains with narrow distributions of the thickness (modal values, 2.97 and 3.94 nm) and diagonal size (1.51 μm). The crystallinity of the graphdiyne nanosheet was confirmed by 2D GIWAXS, revealing its ABC stacking, identical to multilayer graphdiyne produced at the liquid/liquid interface. The in-plane and out-of-plane periodicities were determined to be $a = b = 0.96$ nm and $c = 1.02$ nm, respectively. The c value corresponds to an interlayer distance of 0.34 nm. The XPS and Raman spectra of the graphdiyne nanosheet were consistent with the chemical structure and bonding of graphdiyne, and it did possess a much lower oxygen/carbon ratio (0.09) than either multilayer graphdiyne produced at the liquid/liquid interface (0.21) or bulk graphdiyne synthesized in a single-phase reaction (~0.2). Therefore, the well-defined regular hexagonal domain shape with narrow domain size and thickness distributions was reflected in the good crystallinity and low oxygenic defect level of the few-layer graphdiyne nanosheet.

EXPERIMENTAL SECTION

Materials. All chemicals were purchased from Tokyo Chemical Industry Co., Ltd., Kanto Chemical Co., or Wako Pure Chemical Industries, Ltd., unless otherwise stated. They were used without further purification. Water was purified using a Milli-Q purification system (Merck KGaA). A Si(100) wafer covered with an 85 nm SiO_2 layer was purchased from Electronics and Materials Corp., Ltd. and hydrophobized using HMDS as follows. The Si substrate was placed into a desiccator with HMDS (0.1 mL). The desiccator was then purged with argon and left to stand overnight. The hydrophobized substrate was dried in vacuo overnight and stored under argon. A molybdenum TEM grid with a mesh size of 100 μm and a copper grid covered with an elastic carbon matrix were purchased from Okenshoji Co., Ltd., and a grid with a holey carbon matrix was purchased from Alliance Biosystems, Inc. Hexakis[(trimethylsilyl)ethynyl]benzene was synthesized according to a previous method.[67]

Instruments. Optical microscope images were taken using a VHX-100 (Keyence Corp). FE-SEM images were collected using a JEOL JSM-7400FNT equipped with an EDS analyzer (JEOL EX-2300). The TEM images/SAED patterns in Figures 2e,f,h, 4c, and S1a (SI) were recorded at an accelerating voltage of 75 kV using a HITACHI HF-2000 equipped with an AMT-CCD camera, while the image in Figure S4d (SI) was at an accelerating voltage of 60 kV using a JEM-2010F equipped with a CEOS postspecimen spherical aberration corrector. XPS data were acquired using an ULVAC-PHI PHI 5000 VersaProbe spectrometer. Al Kα (15 kV, 25 W) radiation was used as the X-ray source, and the beam was focused on a 100 μm^2 area. The spectra were analyzed using MultiPak Software and standardized using the Si 2p peak (originating from SiO_2) at 103.3 eV. Raman spectra were collected using a JASCO NRS-1000 (laser wavelength, 532 nm). AFM measurements were carried out using an Agilent Technologies 5500 scanning probe microscope under ambient conditions in the high-amplitude mode (tapping mode) with a silicon cantilever Nano World NCH probe. Synchrotron two-dimensional wide-angle X-ray scattering (2D GIWAXS) experiments were performed at BL45XU in SPring-8 (RIKEN, Hyogo, Japan). The X-ray wavelength and the sample-to-detector distance were, respectively, 1.0 Å and 361 mm. Diffractions from a sample were detected using a Pilatus3X 2 M detector. Recorded diffraction images were integrated along the Debye−Scherrer ring using FIT2D software,[68] affording a one-dimensional intensity profile.

DOI: 10.1021/jacs.6b12776
J. Am. Chem. Soc. 2017, 139, 3145−3152

Preparation of HEB.[61] *Caution! HEB is highly sensitive and explosive; therefore, it must be handled with care! Concentrated solution and solidified phases must be avoided.* All synthetic procedures were conducted under an argon atmosphere in the dark. To a solution of hexakis[(trimethylsilyl)ethynyl]benzene[67] (0.66 mg, 1 μmol) in dichloromethane (10 mL) was added tetrabutylammonium fluoride (1 M in 10 μL of THF, 10 μmol). The solution was shaken for 10 min to obtain HEB (0.1 mM in dichloromethane). The solution was immediately used for the synthesis of graphdiyne without further purification because of its instability.

Synthesis of Multilayer Graphdiyne via a Liquid/Liquid Interfacial Reaction. Under an argon atmosphere at room temperature, a dichloromethane solution of HEB (0.1 mM, 10 mL) was poured into a glass cylinder with a diameter of 35 mm. The solution was then covered with pure water (10 mL) such that a two-phase system was formed. An aqueous solution (10 mL) of copper acetate (0.01 M) and pyridine (0.25 M) was added gently to the water phase. The reaction system was kept undisturbed for 24 h, and a brown film of graphdiyne was generated at the interface. The aqueous layer was then replaced with aqueous HCl (1 M) and then pure water, while the organic layer was replaced with pure dichloromethane. After the removal of both aqueous and organic phases, the resultant graphdiyne film was suspended in ethanol. The suspension was cast dropwise on various substrates.

Synthesis of Few-Layer Graphdiyne via a Gas/Liquid Interfacial Reaction. Under an argon atmosphere at room temperature, an aqueous solution (10 mL) of copper(II) acetate (0.01 M) and pyridine (0.02 M) was poured into the glass cylinder. Onto the surface of this solution was sprayed gently pure toluene (200 μL). Then the HEB–dichloromethane solution (0.1 mM, 20 μL) was sprinkled in the same manner. The screw cap of the cylinder was then closed loosely such that the organic solvent evaporated spontaneously over 24 h. This series of processes resulted in the formation of a few-layer graphdiyne nanosheet on the surface of the aqueous phase. The obtained sheet was deposited on a Si substrate by bringing the substrate close to the interface in the horizontal direction (Langmuir–Schäfer method).

SAED and 2D GIWAXS Simulation. To reproduce the obtained SAED and 2D GIWAXS patterns (Figures 2f and 5b), three types of 3D lattices comprising piles of single-layer graphdiyne were considered. The three lattices include AA-, AB-, and ABC-stack models, because 6-fold symmetry is required to reproduce the hexagonal diffraction pattern in SAED. First, the atomic arrangement of single-layer graphdiyne was optimized using density-functional theory implemented in an ABINIT software package[69] with a projector-augmented-wave method.[70] We employed the generalized gradient approximation of the Perdew–Burke–Ernzerhof exchange–correlation functional,[71] and the kinetic energy cutoff was chosen to be 400 eV. The optimization was performed with convergence criteria for the atomic forces (<0.01 eV/Å) and total energy ($<10^{-5}$ eV) in the self-consistent field iteration. The optimized cell was then expanded by 1.5% to reproduce the observed diffraction data. The AA-, AB-, and ABC-stack models were then constructed by piling the single-layer model, with a parallel displacement of $^1/_3(2a + b)$, for the AB-stack structure, and those of $^1/_3(2a + b)$ and $^1/_3(a + 2b)$ for the ABC-stack structures. The SAED and 2D GIWAXS patterns were simulated using CrystalMaker 2.6.3, SingleCrystal 2.3, and CrystalDiffract 6.5.5 (CrystalMaker Software Ltd.).

AFM-Based Size Analysis of Few-Layer Graphdiyne. The thickness of each hexagonal domain was determined by taking the difference between the average heights of the sheet and bare substrate in a line profile. The lateral size was determined by counting the number of pixels of a sheet in the AFM topograph.

■ ASSOCIATED CONTENT

Supporting Information

The Supporting Information is available free of charge on the ACS Publications website at DOI: 10.1021/jacs.6b12776.

TEM/SAED simulation, optical micrograph, additional SEM, TEM, and AFM images, and 2D GIWAXS simulation for few-layer graphdiyne (PDF)

CIF files for the simulated AA stacking lattice (CIF)

CIF files for the simulated AB stacking lattice (CIF)

CIF files for the simulated ABC stacking lattice (CIF)

■ AUTHOR INFORMATION

Corresponding Authors

*sakamoto@chem.s.u-tokyo.ac.jp

*nisihara@chem.s.u-tokyo.ac.jp

ORCID

Ryota Sakamoto: 0000-0002-8702-1378

Notes

The authors declare no competing financial interest.

■ ACKNOWLEDGMENTS

The present paper was supported by JST-PRESTO "Hyper-nano-space design toward Innovative Functionality" (To R.S.) and JST-CREST "Development of Atomic or Molecular Two-Dimensional Functional Films and Creation of Fundamental Technologies for Their Applications" (to H.N.). This work was also supported by JSPS KAKENHI Grant Numbers JP16H00900, JP25107001, JP25107004, JP15H00862, JP26708005, JP26220801, JP16H00957, JP16H04343, and JP16K14446. The synchrotron radiation experiments were performed at BL45XU in SPring-8 with the approval of RIKEN (Proposal No. 20160041). We acknowledge Dr. Zheng Liu (AIST, Japan) for the TEM image in Figure S4d (SI). The authors acknowledge the Research Hub Advanced Nano Characterization (Graduate School of Engineering, The University of Tokyo) for the XPS study.

■ REFERENCES

(1) Payamyar, P.; King, B. T.; Öttinger, H. C.; Schlüter, A. D. *Chem. Commun.* **2016**, *52*, 18–34.

(2) Sakamoto, J.; van Heijst, J.; Lukin, O.; Schlüter, A. D. *Angew. Chem., Int. Ed.* **2009**, *48*, 1030–1069.

(3) Sakamoto, R.; Takada, K.; Sun, X.; Pal, T.; Tsukamoto, T.; Phua, E. J. H.; Rapakousiou, A.; Hoshiko, K.; Nishihara, H. *Coord. Chem. Rev.* **2016**, *320–321*, 118–128.

(4) Boott, C. E.; Nazemi, A.; Manners, I. *Angew. Chem., Int. Ed.* **2015**, *54*, 13876–13894.

(5) Amo-Ochoa, P.; Welte, L.; González-Prieto, R.; Sanz Miguel, P. J.; Gómez-García, C. J.; Mateo-Martí, E.; Delgado, S.; Gómez-Herrero, J.; Zamora, F. *Chem. Commun.* **2010**, *46*, 3262.

(6) Hermosa, C.; Horrocks, B. R.; Martínez, J. I.; Liscio, F.; Gómez-Herrero, J.; Zamora, F. *Chem. Sci.* **2015**, *6*, 2553–2558.

(7) Tan, J.-C.; Saines, P. J.; Bithell, E. G.; Cheetham, A. K. *ACS Nano* **2012**, *6*, 615–621.

(8) Gallego, A.; Hermosa, C.; Castillo, O.; Berlanga, I.; Gómez-García, C. J.; Mateo-Martí, E.; Martínez, J. I.; Flores, F.; Gómez-Navarro, C.; Gómez-Herrero, J.; Delgado, S.; Zamora, F. *Adv. Mater.* **2013**, *25*, 2141–2146.

(9) Michl, J.; Magnera, T. F. *Proc. Natl. Acad. Sci. U. S. A.* **2002**, *99*, 4788–4792.

(10) Perepichka, D. F.; Rosei, F. *Science* **2009**, *323*, 216–217.

(11) Colson, J. W.; Dichtel, W. R. *Nat. Chem.* **2013**, *5*, 453–465.

(12) Mattevi, C.; Kim, H.; Chhowalla, M. *J. Mater. Chem.* **2011**, *21*, 3324–3334.

(13) Yu, J.; Li, J.; Zhang, W.; Chang, H. *Chem. Sci.* **2015**, *6*, 6705–6716.

DOI: 10.1021/jacs.6b12776
J. Am. Chem. Soc. 2017, 139, 3145–3152

(14) Lin, S.; Diercks, C. S.; Zhang, Y.-B.; Kornienko, N.; Nichols, E. M.; Zhao, Y.; Paris, A. R.; Kim, D.; Yang, P.; Yaghi, O. M.; Chang, C. J. *Science* **2015**, *349*, 1208−1213.
(15) Jin, S.; Supur, M.; Addicoat, M.; Furukawa, K.; Chen, L.; Nakamura, T.; Fukuzumi, S.; Irle, S.; Jiang, D. *J. Am. Chem. Soc.* **2015**, *137*, 7817−7827.
(16) Segura, J. L.; Mancheño, M. J.; Zamora, F. *Chem. Soc. Rev.* **2016**, *45*, 5635−5671.
(17) Dmitriev, A.; Spillmann, H.; Lin, N.; Barth, J. V.; Kern, K. *Angew. Chem., Int. Ed.* **2003**, *42*, 2670−2673.
(18) Stepanow, S.; Lingenfelder, M.; Dmitriev, A.; Spillmann, H.; Delvigne, E.; Lin, N.; Deng, X.; Cai, C.; Barth, J. V.; Kern, K. *Nat. Mater.* **2004**, *3*, 229−233.
(19) Zwaneveld, N. a a; Pawlak, R.; Abel, M.; Catalin, D.; Gigmes, D.; Bertin, D.; Porte, L. *J. Am. Chem. Soc.* **2008**, *130*, 6678−6679.
(20) Tanoue, R.; Higuchi, R.; Enoki, N.; Miyasato, Y.; Uemura, S.; Kimizuka, N.; Stieg, A. Z.; Gimzewski, J. K.; Kunitake, M. *ACS Nano* **2011**, *5*, 3923−3929.
(21) Kambe, T.; Sakamoto, R.; Hoshiko, K.; Takada, K.; Miyachi, M.; Ryu, J.-H.; Sasaki, S.; Kim, J.; Nakazato, K.; Takata, M.; Nishihara, H. *J. Am. Chem. Soc.* **2013**, *135*, 2462−2465.
(22) Kambe, T.; Sakamoto, R.; Kusamoto, T.; Pal, T.; Fukui, N.; Hoshiko, K.; Shimojima, T.; Wang, Z.; Hirahara, T.; Ishizaka, K.; Hasegawa, S.; Liu, F.; Nishihara, H. *J. Am. Chem. Soc.* **2014**, *136*, 14357−14360.
(23) Sakamoto, R.; Hoshiko, K.; Liu, Q.; Yagi, T.; Nagayama, T.; Kusaka, S.; Tsuchiya, M.; Kitagawa, Y.; Wong, W.-Y.; Nishihara, H. *Nat. Commun.* **2015**, *6*, 6713.
(24) Rodenas, T.; Luz, I.; Prieto, G.; Seoane, B.; Miro, H.; Corma, A.; Kapteijn, F.; Llabrés i Xamena, F. X.; Gascon, J. *Nat. Mater.* **2014**, *14*, 48−55.
(25) Takada, K.; Sakamoto, R.; Yi, S.-T.; Katagiri, S.; Kambe, T.; Nishihara, H. *J. Am. Chem. Soc.* **2015**, *137*, 4681−4689.
(26) Huang, X.; Sheng, P.; Tu, Z.; Zhang, F.; Wang, J.; Geng, H.; Zou, Y.; Di, C.; Yi, Y.; Sun, Y.; Xu, W.; Zhu, D. *Nat. Commun.* **2015**, *6*, 7408.
(27) Makiura, R.; Motoyama, S.; Umemura, Y.; Yamanaka, H.; Sakata, O.; Kitagawa, H. *Nat. Mater.* **2010**, *9*, 565−571.
(28) Bauer, T.; Zheng, Z.; Renn, A.; Enning, R.; Stemmer, A.; Sakamoto, J.; Schlüter, A. D. *Angew. Chem., Int. Ed.* **2011**, *50*, 7879−7884.
(29) Dai, W.; Shao, F.; Szczerbiński, J.; McCaffrey, R.; Zenobi, R.; Jin, Y.; Schlüter, A. D.; Zhang, W. *Angew. Chem., Int. Ed.* **2016**, *55*, 213−217.
(30) Grill, L.; Dyer, M.; Lafferentz, L.; Persson, M.; Peters, M. V.; Hecht, S. *Nat. Nanotechnol.* **2007**, *2*, 687−691.
(31) Lafferentz, L.; Eberhardt, V.; Dri, C.; Africh, C.; Comelli, G.; Esch, F.; Hecht, S.; Grill, L. *Nat. Chem.* **2012**, *4*, 215−220.
(32) Bieri, M.; Treier, M.; Cai, J.; Aït-Mansour, K.; Ruffieux, P.; Gröning, O.; Gröning, P.; Kastler, M.; Rieger, R.; Feng, X.; Müllen, K.; Fasel, R. *Chem. Commun.* **2009**, 6919.
(33) Bieri, M.; Nguyen, M.-T.; Gröning, O.; Cai, J.; Treier, M.; Aït-Mansour, K.; Ruffieux, P.; Pignedoli, C. A.; Passerone, D.; Kastler, M.; Müllen, K.; Fasel, R. *J. Am. Chem. Soc.* **2010**, *132*, 16669−16676.
(34) Bieri, M.; Blankenburg, S.; Kivala, M.; Pignedoli, C. a; Ruffieux, P.; Müllen, K.; Fasel, R. *Chem. Commun.* **2011**, *47*, 10239.
(35) Gutzler, R.; Walch, H.; Eder, G.; Kloft, S.; Heckl, W. M.; Lackinger, M. *Chem. Commun.* **2009**, 4456.
(36) Eichhorn, J.; Strunskus, T.; Rastgoo-Lahrood, A.; Samanta, D.; Schmittel, M.; Lackinger, M. *Chem. Commun.* **2014**, *50*, 7680.
(37) Eichhorn, J.; Nieckarz, D.; Ochs, O.; Samanta, D.; Schmittel, M.; Szabelski, P. J.; Lackinger, M. *ACS Nano* **2014**, *8*, 7880−7889.
(38) Abel, M.; Clair, S.; Ourdjini, O.; Mossoyan, M.; Porte, L. *J. Am. Chem. Soc.* **2011**, *133*, 1203−1205.
(39) Koudia, M.; Abel, M. *Chem. Commun.* **2014**, *50*, 8565.
(40) Blunt, M. O.; Russell, J. C.; Champness, N. R.; Beton, P. H. *Chem. Commun.* **2010**, *46*, 7157.
(41) Russell, J. C.; Blunt, M. O.; Garfitt, J. M.; Scurr, D. J.; Alexander, M.; Champness, N. R.; Beton, P. H. *J. Am. Chem. Soc.* **2011**, *133*, 4220−4223.
(42) Peyrot, D.; Silly, F. *ACS Nano* **2016**, *10*, 5490−5498.
(43) Morchutt, C.; Björk, J.; Krotzky, S.; Gutzler, R.; Kern, K. *Chem. Commun.* **2015**, *51*, 2440−2443.
(44) Zhang, Y.-Q.; Kepčija, N.; Kleinschrodt, M.; Diller, K.; Fischer, S.; Papageorgiou, A. C.; Allegretti, F.; Björk, J.; Klyatskaya, S.; Klappenberger, F.; Ruben, M.; Barth, J. V. *Nat. Commun.* **2012**, *3*, 1286.
(45) Klappenberger, F.; Zhang, Y.-Q.; Björk, J.; Klyatskaya, S.; Ruben, M.; Barth, J. V. *Acc. Chem. Res.* **2015**, *48*, 2140−2150.
(46) Sun, Q.; Cai, L.; Ma, H.; Yuan, C.; Xu, W. *ACS Nano* **2016**, *10*, 7023−7030.
(47) Kissel, P.; Erni, R.; Schweizer, W. B.; Rossell, M. D.; King, B. T.; Bauer, T.; Götzinger, S.; Schlüter, A. D.; Sakamoto, J. *Nat. Chem.* **2012**, *4*, 287−291.
(48) Kory, M. J.; Wörle, M.; Weber, T.; Payamyar, P.; van de Poll, S. W.; Dshemuchadse, J.; Trapp, N.; Schlüter, A. D. *Nat. Chem.* **2014**, *6*, 779−784.
(49) Kissel, P.; Murray, D. J.; Wulftange, W. J.; Catalano, V. J.; King, B. T. *Nat. Chem.* **2014**, *6*, 774−778.
(50) Payamyar, P.; Kaja, K.; Ruiz-Vargas, C.; Stemmer, A.; Murray, D. J.; Johnson, C. J.; King, B. T.; Schiffmann, F.; VandeVondele, J.; Renn, A.; Götzinger, S.; Ceroni, P.; Schütz, A.; Lee, L.; Zheng, Z.; Sakamoto, J.; Schlüter, A. D. *Adv. Mater.* **2014**, *26*, 2052−2058.
(51) Murray, D. J.; Patterson, D. D.; Payamyar, P.; Bhola, R.; Song, W.; Lackinger, M.; Schlüter, A. D.; King, B. T. *J. Am. Chem. Soc.* **2015**, *137*, 3450−3453.
(52) Lange, R. Z.; Hofer, G.; Weber, T.; Schlüter, A. D. *J. Am. Chem. Soc.* DOI: 10.1021/jacs.6b11857.
(53) Eck, W.; Küller, A.; Grunze, M.; Völkel, B.; Gölzhäuser, A. *Adv. Mater.* **2005**, *17*, 2583−2587.
(54) Turchanin, A.; Gölzhäuser, A. *Adv. Mater.* **2016**, *28*, 6075−6103.
(55) Schrettl, S.; Stefaniu, C.; Schwieger, C.; Pasche, G.; Oveisi, E.; Fontana, Y.; Morral, A. F. i; Reguera, J.; Petraglia, R.; Corminboeuf, C.; Brezesinski, G.; Frauenrath, H. *Nat. Chem.* **2014**, *6*, 468−476.
(56) Li, Y.; Xu, L.; Liu, H.; Li, Y. *Chem. Soc. Rev.* **2014**, *43*, 2572.
(57) Li, G.; Li, Y.; Liu, H.; Guo, Y.; Li, Y.; Zhu, D. *Chem. Commun.* **2010**, *46*, 3256.
(58) Li, G.; Li, Y.; Qian, X.; Liu, H.; Lin, H.; Chen, N.; Li, Y. *J. Phys. Chem. C* **2011**, *115*, 2611−2615.
(59) Qian, X.; Ning, Z.; Li, Y.; Liu, H.; Ouyang, C.; Chen, Q.; Li, Y. *Dalton Trans.* **2012**, *41*, 730−733.
(60) Qian, X.; Liu, H.; Huang, C.; Chen, S.; Zhang, L.; Li, Y.; Wang, J.; Li, Y. *Sci. Rep.* **2015**, *5*, 7756.
(61) Zhou, J.; Gao, X.; Liu, R.; Xie, Z.; Yang, J.; Zhang, S.; Zhang, G.; Liu, H.; Li, Y.; Zhang, J.; Liu, Z. *J. Am. Chem. Soc.* **2015**, *137*, 7596−7599.
(62) Eglinton, G.; Galbraith, A. R. *J. Chem. Soc.* **1959**, 889.
(63) Long, M.; Tang, L.; Wang, D.; Li, Y.; Shuai, Z. *ACS Nano* **2011**, *5*, 2593−2600.
(64) Luo, G.; Zheng, Q.; Mei, W.-N.; Lu, J.; Nagase, S. *J. Phys. Chem. C* **2013**, *117*, 13072−13079.
(65) Bae, S.; Kim, H.; Lee, Y.; Xu, X.; Park, J.-S.; Zheng, Y.; Balakrishnan, J.; Lei, T.; Ri Kim, H.; Song, Y. I.; Kim, Y.-J.; Kim, K. S.; Özyilmaz, B.; Ahn, J.-H.; Hong, B. H.; Iijima, S. *Nat. Nanotechnol.* **2010**, *5*, 574−578.
(66) Gao, G.; Liu, D.; Tang, S.; Huang, C.; He, M.; Guo, Y.; Sun, X.; Gao, B. *Sci. Rep.* **2016**, *6*, 20034.
(67) Sonoda, M.; Inaba, A.; Itahashi, K.; Tobe, Y. *Org. Lett.* **2001**, *3*, 2419−2421.
(68) Hammersley, A. P. *FIT2D: An Introduction and Overview*; ESRF97HA02T; ESRF Internal Report: Grenoble, France, February 1997.
(69) Gonze, X.; Amadon, B.; Anglade, P.-M.; Beuken, J.-M.; Bottin, F.; Boulanger, P.; Bruneval, F.; Caliste, D.; Caracas, R.; Côté, M.; Deutsch, T.; Genovese, L.; Ghosez, P.; Giantomassi, M.; Goedecker, S.; Hamann, D. R.; Hermet, P.; Jollet, F.; Jomard, G.; Leroux, S.;

DOI: 10.1021/jacs.6b12776
J. Am. Chem. Soc. 2017, 139, 3145−3152

Mancini, M.; Mazevet, S.; Oliveira, M. J. T.; Onida, G.; Pouillon, Y.; Rangel, T.; Rignanese, G.-M.; Sangalli, D.; Shaltaf, R.; Torrent, M.; Verstraete, M. J.; Zerah, G.; Zwanziger, J. W. *Comput. Phys. Commun.* **2009**, *180*, 2582−2615.
(70) Torrent, M.; Jollet, F.; Bottin, F.; Zérah, G.; Gonze, X. *Comput. Mater. Sci.* **2008**, *42*, 337−351.
(71) Perdew, J. P.; Burke, K.; Ernzerhof, M. *Phys. Rev. Lett.* **1996**, *77*, 3865−3868.

DOI: 10.1021/jacs.6b12776
J. Am. Chem. Soc. 2017, 139, 3145−3152